THE COMPARISON OF ELECTROCHEMICAL IMPEDANCE BEHAVIORS OF LITHIUM-ION AND NICKEL-METAL HYDRIDE BATTERIES AT DIFFERENT STATE-OF-CHARGE CONDITIONS

Uğur MORALI[1] , Salim EROL[2*]

[1]Eskişehir Osmangazi Üniversitesi, Mühendislik ve Mimarlık Fakültesi, Kimya Mühendisliği Bölümü, Eskişehir
ORCID No : http://orcid.org/0000-0001-7794-6943
[2]Eskişehir Osmangazi Üniversitesi, Mühendislik ve Mimarlık Fakültesi, Kimya Mühendisliği Bölümü, Eskişehir
ORCID No : http://orcid.org/0000-0002-7219-6642

Keywords
Li-ion battery
Ni-MH battery
Impedance spectroscopy
State of Charge
Equivalent circuit model

Abstract

In this study, impedance responses of a lithium-ion battery and a nickel metal-hydride battery were analyzed as a function of different state of charge conditions. The physical parameters of these widely used rechargeable batteries have been extracted through an equivalent circuit model by fitting impedance data. The fit was excellent. The regressed parameters explain the battery physics and dynamics well. Results show that the developed model could be utilized for the broadly used rechargeable batteries at their operational potentials. The electrochemical impedance spectroscopy is a beneficial technique to provide information regarding battery life, battery performance, and state of health of a battery.

LİTYUM İYON VE NİKEL METAL HİDRİT PİLİNİN FARKLI ŞARJ DURUMLARINDA ELEKTROKİMYASAL EMPEDANS DAVRANIŞININ KARŞILAŞTIRILMASI

Anahtar Kelimeler
Li-iyon pil
Ni-MH pil
Empedans spektroskopisi
Şarj durumu
Eşdeğer devre modeli

Öz

Bu çalışmada, bir lityum-iyon pili ve bir nikel metal hidrit pilinin empedans cevapları farklı şarj durumlarının bir fonksiyonu olarak analiz edilmiştir. Oldukça yaygın olarak kullanılan tekrar şarj edilebilir bu pillere ait fiziksel parametreler empedans verilerinin eşdeğer devre modeline uymasıyla elde edilmiştir. Model ile veriler mükemmel bir şekilde uyum göstermişlerdir. Regresyon analizi ile elde edilen parametreler bataryaların durumunu ve dinamiklerini iyi bir şekilde açıklamaktadır. Sonuçlar geliştirilen modelin tekrar şarj edilebilir pillerin çalışma potansiyelleri için kullanılabileceğini göstermektedir. Elektrokimyasal empedans spektroskopisi batarya ömrü, batarya performansı ve bataryanın fayda durumu ile ilgili bilgiler veren faydalı bir tekniktir.

Araştırma Makalesi		Research Article	
Başvuru Tarihi	: 05.07.2019	Submission Date	: 05.07.2019
Kabul Tarihi	: 04.11.2019	Accepted Date	: 04.11.2019

1. Introduction

In recent years, to reduce the dependence on conventional energy sources, electric vehicles and hybrid electric vehicles are considered as the most popular technologies. These technologies also provide a solution to the environmental problems caused by transportation (Jaguemont, Boulon, & Dube, 2016a). The energy storage systems, especially batteries, are the most significant part of these technological systems (Jaguemont, Boulon, & Dube, 2016b). The applications of the battery rank among the most important systems of the world. Batteries are used in mobile phones, portable devices, hybrid and electric vehicles, and modern aircrafts. The types of the application determine battery dimension, battery capacity, power and energy density (Fleischer, Waag, Heyn, & Sauer, 2014). It is important to recognize the battery capacity and its power density to conserve the battery performance during the operation and to get a longer cell life (Galeotti, Cinà, Giammanco, Cordiner, & Di Carlo, 2015).

A battery package typically consists of a negative electrode, electrolyte, a separator, current collectors, and a positive electrode. Several processes such as electrochemical reactions and mass transport occur when the battery is in operation. These processes determine the battery performance and remaining useful life, which can be considered as state of health of the battery (Leng, Wei, Tan, & Yazami, 2017). Different kinds of methods were developed by the scientists and researchers to understand these processes in the

* Sorumlu yazar; e-posta : esalim@ogu.edu.tr

battery (Ecker et al., 2015). One of these methods is electrochemical impedance spectroscopy (EIS) that is widely used to specify electrochemical processes and to determine their effects (Xie, Li, & Yuan, 2014). EIS is a measurement technique based on alternating potential or current at various frequencies. It is possible to evaluate the physical and chemical properties in a battery without any destruction by using EIS (Ecker et al., 2015; Galeotti et al., 2015; Huang, Li, Liaw, & Zhang, 2016). Impedance analysis could be made by plotting different types of diagnostic graphs. There are two main plots, namely Nyquist plot and Bode plot. These plots are used to provide valuable information on the key performance parameters of a battery. Nyquist plots of batteries generally display a vertical line at high frequencies, semi-circles or depressed semi-circles at mid-frequencies, and a slopped line or curve at low frequencies (Raijmakers, Danilov, van Lammeren, Lammers, & Notten, 2014). These frequency regions of the Nyquist plot provide information for ohmic resistance at high frequencies, charge transfer resistance and double layer capacitance at mid-frequencies, diffusion of the ions through electrolyte/electrode interphase at low frequencies (Itagaki, Honda, Hoshi, & Shitanda, 2015). To obtain battery parameters, a model that simulates characteristics of a battery was applied to the EIS data (Castano-Solis, Serrano-Jimenez, Gauchia, & Sanz, 2017). The battery models are designed as an equivalent circuit consisting of various kinds of elements such as electrolyte resistances, capacitances, inductances, charge transfer resistances, constant phase elements, Warburg elements, and so on. The configuration of the elements in the equivalent circuit influences the accuracy and stability of the model (Leng et al., 2017).

The impact of connecting cells in parallel on the energy imbalance was investigated by Bruen and Marco (Bruen & Marco, 2016). They used a validated model against EIS data for four 3 Ah 18650 lithium ion cells. Gong et al. studied the characteristics of battery packs with parallel-connected lithium-ion battery cells (Gong, Xiong, & Mi, 2015). Various battery packs were built with a group of degraded lithium-ion cells to explore the effect of the cell consistency in parallel-connected cells. This was achieved through the physical model simulating the operation of the battery packs. In another study, Ecker et al. studied on 7.5 Ah lithium-ion cell to determine the physical parameters through a electrochemical model (Ecker et al., 2015). The measured parameters were compared with the model results. In a different study, Hang et al. measured the impedance of the lithium-ion battery with $Li_4Ti_5O_{12}$ anode at different states of charge and temperatures (Hang et al., 2013). They determined the reason of the capacity fade of the lithium-ion battery by using equivalent circuit model. They showed that the equivalent circuit model could be used for interpretation of the performance parameters of the battery. Gomez et al. proposed an equivalent circuit model for a Sony commercial Li-ion polymer battery at several states of charges (Gomez, Nelson, Kalu, Weatherspoon, & Zheng, 2011). Their model had a quite number of parameters including multiple double layer capacitances, charge transfer resistances, an inductance, a Warburg impedance, and an intercalation capacitance to fit the EIS data they collected. Cruz et al. analyzed the impedance spectroscopy of nickel metal hydride (Ni-MH) batteries at different SoC with a proposed equivalent circuit (Cruz-Manzo, Greenwood, & Chen, 2017). They model impedance response based on fundamental electrochemical theories and diffusion mechanisms. Nelatury and Singh suggested two different circuits to fit Ni-MH battery impedance (Nelatury & Singh, 2004). They inserted a Warburg element to the equivalent circuit model when SoC the battery gets lower. In a previous work, Morali and Erol analyzed and modeled the impedance response of commercial Li-ion and Ni-MH batteries at the same cell potential (Moralı & Erol, 2020). A number of models have been developed to characterize and simulate lithium-ion and nickel metal hydride cells. These models have already described the battery systems. However, they have been only valid for the modelled system. Further equivalent circuits can be improved for a recognized model simulating every types of battery.

The objective of this study is to introduce an effective model appropriate for through analysis of performance parameters of both Li-ion cell and Ni-MH battery. This was achieved through EIS method that was applied to commercially available 18650 Li-ion cells and 6HR61 Ni-MH cells at various SoC conditions. The contribution of this study is to extend the existing literature in terms of both simulation method and experimental data.

2. Materials and Methods

Electrochemical experiments were performed by a potentiostat on a 18650 Li-ion and a 6HR61 Ni-MH battery cells.

2.1. Materials

Experiments were carried out on commercial cylindrical 18650 lithium-ion cells (diameter: 18 mm, length: 65 mm, weight: 47 g average, capacity: 3000 mAh, Sony VTC6, Sony Energy, Japan) and commercial rectangular 6HR61 Ni-MH cells (horizontal length: 24.5 mm, vertical length: 46.5 mm, thickness: 17.5 mm, typical volume: 22.8 cm^3, weight: 42 g average, capacity: 170 mAh, Duracell 6HR61, Duracell batteries, USA). The tested 18650 Li-ion cells exhibit a working potential between 3.0-4.2 V with a nominal voltage of 3.6V. The vendor supplies a potential range between 7.0-9.2 V for the

6HR61 Ni-MH cell. The tested 6HR61 Ni-MH cell exhibits a nominal potential of 8.4 V. The state of charge of 18650 Li-ion cell and 6HR61 Ni-MH battery was defined as 100% when their potentials reach 4.2 V and 9.2 V, respectively.

2.2 Instruments

All of the electrochemical experiments and impedance measurements were conducted by using a Gamry Reference 3000 Potentiostat/Galvanostat/ZRA from Gamry Instruments, USA. The cylindrical battery holder (Gamry Instruments) for 18650 size cells was used to eliminate additional impedances due to cable connections. Both cells were also placed in a commercial Gamry Faraday cage to prevent environmental magnetic effects on any electrochemical measurements.

2.3. Methods

In this study, research and publication ethics were followed. It is stated in this article that no legal/special permission is required. The state of charge values were calculated based on the integration of time and current, i.e., 0%-100% at the potential window of 3.0 V-4.2 V and 7.0 V-9.2 V for Li-ion cell and NiMH battery, respectively. Prior to the impedance measurements, 18650 Li-ion cell was charged to 4.2 V, and 6HR61 Ni-MH battery was charged to 9.2 V to reach at their 100% state of charge. The batteries were slowly discharged to reach intended SoC values (75%, 50%, 25%, and 0%) after the impedance measurement at fully charged condition. A potentiostatic EIS was conducted from 10 kHz to 10 mHz using a 10 mV ac sinusoidal perturbation at the open circuit potential (OCP) of 18650 Li-ion cell. A galvanostatic EIS measurement was performed on 6HR61 Ni-MH cell in galvanostatic mode from 10 kHz to 10 mHz. Here, the applied for perturbation current was 10 mA. After obtaining impedance data, impedance responses were examined with an equivalent circuit model to extract performance parameters of the batteries. The least-squares method and the Simplex algorithm were employed by using Echem Analyst Software that is connected to the potentiostat.

All of the experiments were performed at room temperature to minimize uncertainty of the results. Gamry software was also activated to reduce errors between the repeated experimental runs.

3. Results

The impedance responses of the 18650 Li-ion cell and 6HR61 Ni-MH cell are presented for 100% state of charge.

3.1 Impedance analysis

To extract the performance parameters of both the 18650 Li-ion cell and 6HR61 Ni-MH battery, the impedance analyses were performed in the frequency range of 100 kHz-10 mHz. The impedance response in Nyquist format for the 18650 Li-ion cell at different SoC is given in Fig. 1. Nyquist diagram shows the negative imaginary part of the impedance as a function of the real part of the impedance of a battery in a frequency range. The distinct electrochemical processes can be indicated by using Nyquist plot (Galeotti et al., 2015). An inductive behavior for 18650 Li-ion cell was determined in the frequency range of 100-2.5 kHz. The inductive behavior, the positive part of the imaginary impedance in Fig. 1, is attributed to result from the interconnections of the cell such as connecting lines and cables (Westerhoff, Kurbach, Lienesch, & Kurrat, 2016). To obtain the data only from the characteristics of a Li-ion cell, the impedance corresponding to 3 kHz can be selected as the highest frequency for the fitting. In the moderate frequency range (2.5 kHz-0.3 Hz), two capacitive loops were observed in Fig. 1. These capacitive loops correspond to the electrochemical reactions occurring in the cell. The first capacitive loop in the higher frequency range of the moderate frequency range indicates the reactions that occur at the negative electrode. The second loop in the lower frequency range corresponds the electrochemical reactions at the positive electrode. The capacitive loops also indicate the formation of the double layer capacitances at the electrolyte/electrode interface and correspond to the charge-transfer processes.

The reactions between Li^+ ions and the constituents in the electrolyte can cause formation of a layer on the negative electrode when the Li-ion cell is in the charge mode. This layer is called solid-electrolyte interphase (SEI). Thus, the charge transfer process can occur both from the electrolyte into the SEI and from the SEI into the electrodes. This additional layer on the negative electrode can cause an increase in the charge transfer resistance of the anode. The SEI layer becomes thicker, and the resistance gets larger while the amount of battery cycle increases. After cycling the battery, the higher charge transfer resistance indicates that the first loop is related to the negative electrode. The lowest frequency region of the impedance curve corresponds to mass transfer of lithium ions between the electrodes and the electrolyte. The slope of the straight line in the lowest frequency region reflects the behavior of the diffusion of ions in the electrode. If the angle between the straight line and the x-axis is 45°, showing that the value of the slope is 1, the diffusion mechanism of the ions in the electrode is given by the Fick's 2nd law of diffusion.

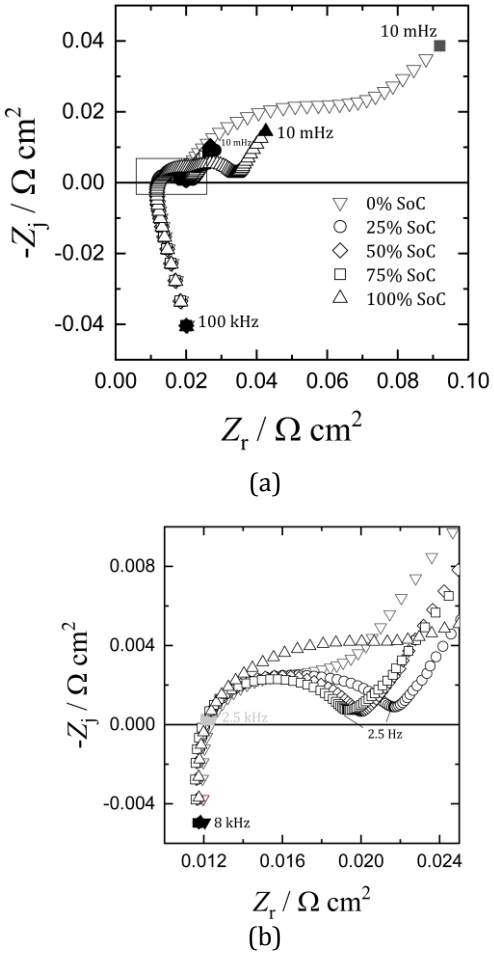

Figure 1. Impedance response of 18650 Li-ion cell at different % SoC: a) complete spectra and b) high frequency values corresponding to the box in (a).

The impedance representation in Nyquist format for 6HR61 Ni-MH at different SoC is shown in Fig. 2. The impedance responses in the higher frequency region between 100 kHz-30 kHz can be attributed to the inductive behavior originated from the inter-connections and cables of the potentiostat. The comparison of the impedance responses of both cells showed that the 6HR61 battery exhibited less inductive behavior in the selected frequency range. This showed that the frequency range between 100 kHz-10 mHz is more suitable for the battery characteristics of the 6HR61 battery. The Nyquist plot in Fig. 2 demonstrates that the impedance of the Ni-MH battery also consists of two capacitive loops as of the Li-ion in the frequency range of 30 kHz-1 Hz. To be consistent with the Li-ion battery impedance behavior, the first loop between 30 kHz-100 Hz is assumed as corresponding to the charge transfer process occurring on the negative electrode that is the oxidation reaction of hydrogen in the negative electrode. The second loop between 100 Hz-1 Hz indicated the electrochemical reaction taking place at positive electrode representing the reduction reaction of NiOOH occurring at the interface of the electrolyte and positive electrode. When the shape of these two loops is compared, it can be deduced that the low frequency loop is not a perfect semicircle. The depressed shape of this loop reflects the heterogeneity of current distribution at the positive electrode surface. The similar assumption was made for the impedance response corresponding to the reaction of the positive electrode in the Li-ion cell. The low frequency impedance can be attributed to the mass transfer of the hydride ions in the cathode. The angle between the straight line and the x-axis at different %SoC is between 45°-48°. This angle range indicated that the diffusion of hydride ions into the cathode could be thought as it obeys the Fick's second law.

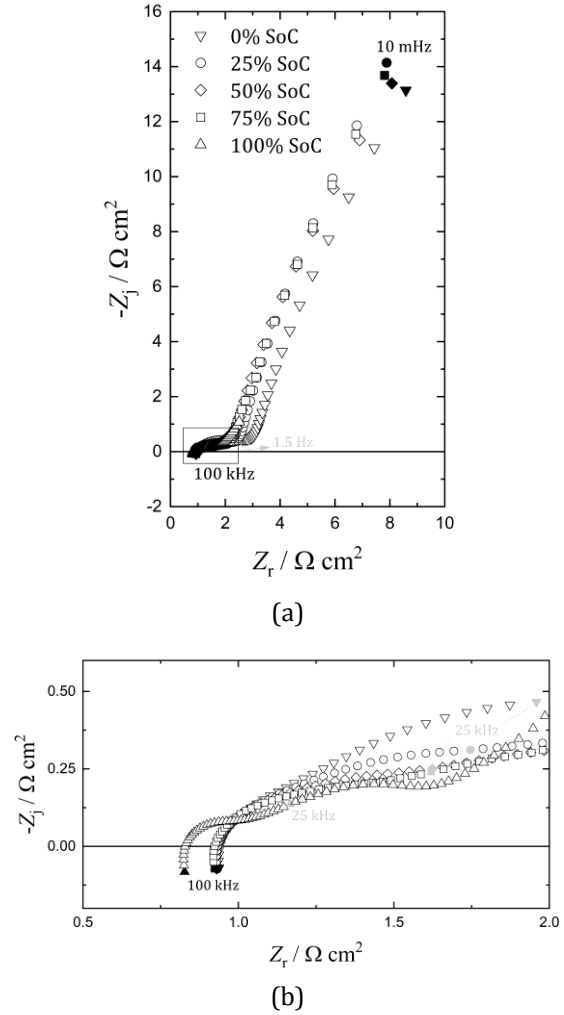

Figure 2. Impedance response of 6HR61 Ni-MH cell at different % SoC: a) complete spectra and b) high frequency values corresponding to the box in (a).

The differences between the impedance responses of these two batteries show distinct electrochemical reaction mechanisms. As shown in Fig. 1 and 2, the comparison of the impedance responses also showed

that the impedance of 6HR61 Ni-MH battery is much greater than that of 18650 Li-ion cell. Present-day technologies enable us high energy density power sources and numerous processes require high energy density energy storage materials. The impedance response of the batteries can provide an insight for the energy density of these energy storage materials. The higher impedance response of the Ni-MH battery implies its lower energy density. This result is in agreement with the energy characteristics of the preferred power sources.

3.2 Mathematical Modeling

Mathematical models are used to describe the characteristics of batteries. These models compose of simple electrical elements. In this section, the equivalent circuit model of the batteries is presented to extract battery dynamics features from the impedance responses.

Equivalent circuit models generally comprise electrical elements such as inductance, resistances, and capacitances. The employed equivalent circuit model for the batteries is shown in Figure 3.

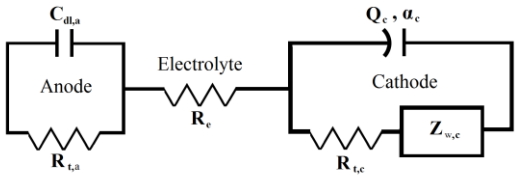

Figure 3. Equivalent circuit model developed for the batteries

The developed equivalent circuit model contains an electrolyte resistance R_e, a charge transfer resistance for negative electrode $R_{t,a}$, a double layer capacitance for anode $C_{dl,a}$, a constant phase element for cathode CPE_c (Q_c, α_c), a charge transfer resistance $R_{t,c}$ and an expression for diffusion in positive electrode $Z_{w,c}$ (Warburg impedance). In this circuit, the impedance response of the resistances of both electrolyte and separator are indicated by the ohmic resistance R_e. The two parallel elements $R_{t,a}$ and $C_{dl,a}$ represent the electrochemical reactions taking place at the negative electrode/electrolyte interface. The constant phase element (CPE) describes the capacity between the electrolyte and the cathode. In the cathode side of the electric circuit, the charge transfer resistance $R_{t,c}$ connected with the $Z_{w,c}$ serially are parallel to the CPE. $R_{t,c}$ represents the resistance of the electrochemical reactions taking place at the electrolyte/positive electrode interface. The CPE presented in Figure 3 indicated by two terms, Q_c and α_c. Q_c is the CPE coefficient associated with the double layer capacitance of the positive electrode. α_c is the CPE exponent that is highly related to a degree of the surface heterogeneity of the electrode. The diffusion of the ions inside the positive electrode is shown by the $Z_{w,c}$ in the equivalent circuit model (Orazem & Tribollet, 2017).

The battery impedance (Z) consists of the main components of the battery, anode (Z_a), electrolyte (R_e) and cathode (Z_c) impedances. Since these impedances are connected in series, the Z value is expressed as the sum of these impedances in Equation 1.

$$Z = Z_a + R_e + Z_c \tag{1}$$

The anodic impedance Z_a in Equation 1 is expressed in Equation 2 as the equivalent impedance of the circuit elements shown in the anode region in Fig. 3.

$$Z_a = \frac{R_{t,a}}{1 + j\omega R_{t,a} C_{dl,a}} \tag{2}$$

The cathodic impedance in Equation 1 is shown in Equation 3, where Z_c is the impedance of the circuit elements shown in the cathode region in Fig. 3.

$$Z_c = \frac{R_{t,c} + Z_{w,c}}{1 + (j\omega)^{\alpha_c}(R_{t,c} + Z_{w,c})Q_c} \tag{3}$$

In equation 4, $Z_{w,c}$ is the Warburg impedance and is defined as

$$Z_{w,c} = \frac{A_{w,c}}{\sqrt{j\omega}} \tag{4}$$

where $A_{w,c}$ is Warburg impedance coefficient and is simply considered as a resistance.

The regression results obtained from equation 1 and the impedance data presented in Fig. 1 are shown in Fig. 4. The regression results obtained from equation 1 and the impedance data presented in Fig. 2 are shown in Fig. 5. The consistency of the model to the impedance responses for both 18650 Li-ion cell and 6HR61 Ni-MH battery is excellent as shown from Fig. 4 and 5. The impedance responses in Fig. 1 and Fig. 2 were fitted to the developed model in Fig. 3 by the Simplex method. The regressed parameters of the model are presented in Table 1.

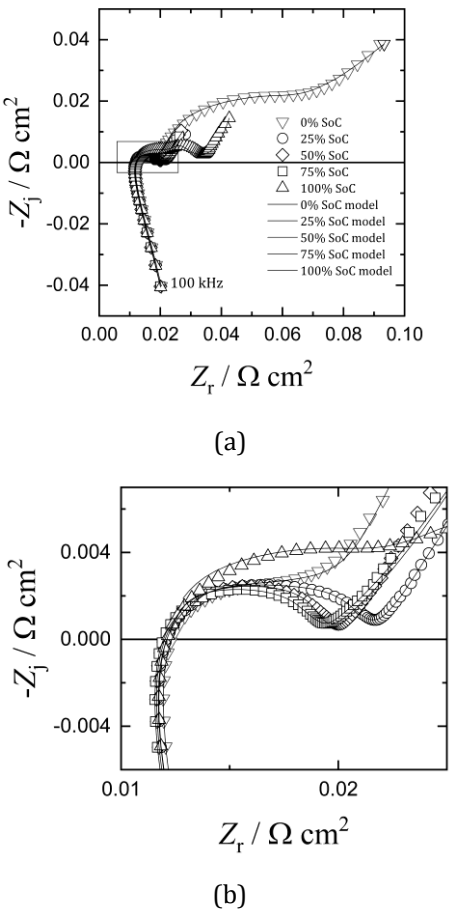

Figure 4. Impedance response of the 18650 Li-ion battery at different SoC values. The straight line represents a fit of the equivalent circuit model using the parameters for Li-ion battery shown in Table 1: a) complete spectra and b) high frequency values corresponding to the box in (a).

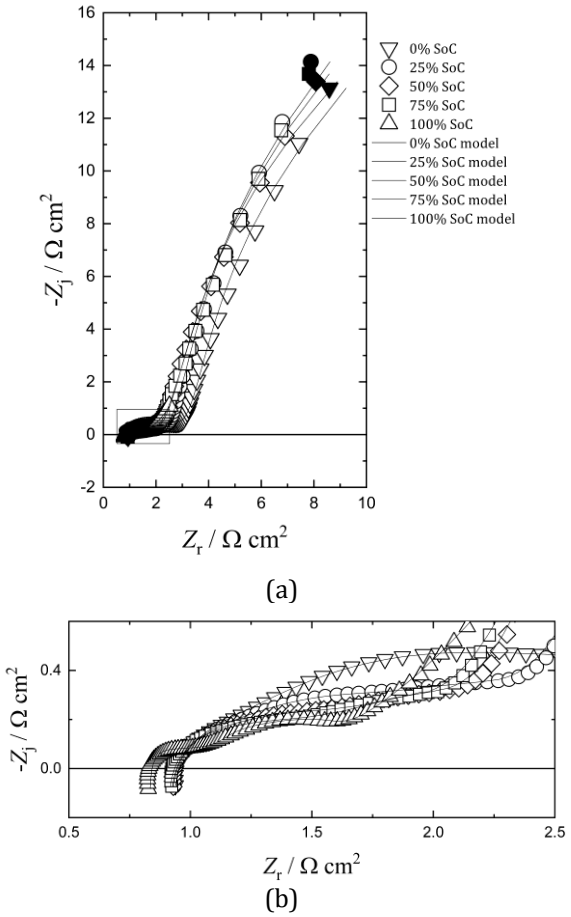

Figure 5. Impedance response of the 6HR61 Ni-MH battery t the different SoC values. The straight line represents a fit of the equivalent circuit model using the parameters for Ni-MH battery shown in Table 1: a) complete spectra and b) low impedance values corresponding to the box in (a).

Table 1
Regression results of equivalent circuit model parameters and their errors

Parameter	100% SoC		75% SoC		50% SoC		25% SoC		0% SoC	
	Li-ion	Ni-MH	Li-ion	Ni-MH	Li-ion	Ni-MH	Li-ion	Ni-MH	Li-ion	Ni-MH
$C_{dl,a}$	2.881±0.2105	0.132±0.0007	421.6±61.38	1.30±0.049	515.2±58.56	0.904±0.0136	469.8±104.4	0.89±0.012	0.163±0.022	0.95±0.014
$R_{t,a}$	0.0115±0.0008	0.6112±0.058	0.0087±0.001	0.756±0.037	0.0068±0.001	0.763±0.146	0.0041±0.0013	0.837±0.028	0.0032±0.0003	0.632±0.015
R_e	0.013±0.0001	0.791±0.0198	0.0012±0.0002	0.89±0.016	0.0012±0.0002	0.810±0.0223	0.0012±0.0002	0.84±0.0175	0.013±0.00013	0.874±0.013
Q_c	2.383±0.4457	0.263±0.058	0.99±0.22	0.043±0.01	0.88±0.203	0.03752±0.008	1.572±0.3255	0.099±0.009	15.72±0.336	0.055±0.004
α_c	0.9191±0.0612	0.337±0.0361	0.87±0.214	0.47±0.03	0.73±0.037	0.304±0.0172	0.6599±0.0352	0.36±0.015	0.52±0.0012	0.423±0.012
$R_{t,c}$	0.008±0.00055	0.5113±0.141	0.0078±0.0003	1.116±0.08	0.0083±0.0003	2.449±0.157	0.0099±0.0004	2.39±0.096	0.115±0.004	2.79±0.071
$A_{w,c}$	2.565±0.3934	2.426±0.115	2.789±0.432	0.89±0.052	2.63±0.323	1.04±0.074	2.79±0.5640	1.12±0.095	0.46±0.021	1.261±0.15

Unit of the equivalent circuit elements $C_{dl,a}$, F cm^{-2}; $R_{t,a}$, Ω cm^2; R_e , Ω cm^2; Q_c , F cm^{-2} s$^{\alpha-1}$; α_c, dimensionless; $R_{t,c}$, Ω cm^2; $A_{w,c}$, Ω cm^2 s$^{1/2}$.

The equivalent circuit model parameter comparison between the 18650 Li-ion and 6HR61 NiMH cells were conducted to indicate the effect of SoC. For the 6HR61 NiMH battery, the anodic resistance was higher than the cathodic resistance when the state-of-charge of the battery was at 100%. This implies that there was no SEI film formation on the anodes or the thickness of this

layer was low. It proves that 6HR61 battery are fresh and was not cycled adequate quantity to form the SEI layer.

For all the %SoC levels, the anodic resistance, the electrolyte resistance and the cathodic resistance for the 6HR61 Ni-MH were higher than those of the 18650 Li-ion cell. The higher ohmic resistance of the Ni-MH battery than that of Li-ion cell indicated that the discharging capacity and the cycling performance was lower than those of the Li-ion cell. Compared with the 6HR61 NiMH battery, the 18650 Li-ion cell had a lower ohmic resistance over the SoC range. Additionally, the lower ohmic resistance of the Li-ion cell was indicative of the higher electrolyte performance. The value of CPE exponent, α, varies between 0.5 and 1 for the electrochemical systems. This parameter for the Li-ion cell is closer to 1 that of the Ni-MH battery. This implies that the current distribution is more uniform and the roughness of the electrode surface is lower in the Li-ion battery. It also indicates that the pores in the cathode exhibited more uniform pore structure. The CPE coefficient, Q_c, is highly related to the capacity of a battery. In other words, the higher value of Q_c represents the higher adsorption ability of the electrode surface for the mobile ions in the electrolyte. Therefore, the Li-ion cell revealed more adsorption capability over the potential range than that of the Ni-MH. The anodic charge transfer resistance of the 18650 Li-ion cell increased with the SoC increasing. This result could be attributed to the thickening SEI layers of the anode resulting higher resistance of Li+ insertion into the electrode. In contrast to the anodic resistance, the cathodic charge transfer resistance of 18650 Li-ion battery decreased in more cases at higher SoC. The cathodic charge transfer resistance of the 6HR61 NiMH battery decreased at higher SoC. However, the dependence of the anodic charge transfer resistance on the SoC could not be observed. The results in Table 1 showed that the cathodic and electrolyte resistances at 0% SoC (low cut-off potential) and 100% SoC (high cut-off potential), reflecting large potential polarization at low and high potentials. The results indicated that the CPE exponent (α) of Li-ion cell increased at higher SoC. Additionally, the higher SoC could provide a uniformly distributed current that is demonstrated as a higher cathodic CPE exponent. The formed SEI layer may provide a uniform electrode surface leading higher α value. Not like the 18650 Li-ion cell, the SoC dependence for the cathodic CPE exponent of 6HR61 NiMH cell was not observed. This could be attributed to the electrolyte solvents and electrode material in the 18650 Li-ion cell different from those in 6HR61 NiMH cell. Although the explanations and fitting models were not exactly conclusive, it can be deduced that the diffusion of the ions in the solid electrode in the low-frequency region was influenced by the electrode structure and composition.

The interpretation of all the results indicates that the Li-ion cell has many advantages over the Ni-MH battery in terms of performance and capacity.

4. Conclusion

The electrochemical impedance analysis was performed on the two rechargeable batteries. An equivalent circuit model was developed that is suitable for both batteries. This study provides useful guides for the interpretation of the impedance responses of both 18650 Li-ion cell and the 6HR61 Ni-MH battery. The applied equivalent circuit analysis can be used for modeling both Li-ion cell and 6HR61 Ni-MH battery, regardless of the chemistry of the cells. The main contribution of this study is that the model can be used to represent the impedance responses and to extract the physically meaningful parameters for Li-ion and Ni-MH batteries throughout operational potential and SoC.

Author Contributions

Uğur Moralı proposed the concept, designed the experiment, carried out the electrochemical work, analyzed the electrochemical data, wrote the manuscript, drew the figures, and discussed the results. Salim Erol jointly conceptualized the paper, developed the methodology, carried out the electrochemical experiments, performed data analysis, wrote the manuscript, discussed the results and reviewed the manuscript.

Acknowledgements

The authors gratefully acknowledge the Eskişehir Osmangazi University Scientific Research Foundation (grant number 2017-1911).

Conflict of Interest

There is no conflict of interest.

References

Bruen, T., & Marco, J. (2016). Modelling and experimental evaluation of parallel connected lithium ion cells for an electric vehicle battery system. *Journal of Power Sources*, 310, 91-101. doi: https://doi.org/10.1016/j.jpowsour.2016.01.001

Castano-Solis, S., Serrano-Jimenez, D., Gauchia, L., & Sanz, J. (2017). The Influence of BMSs on the Characterization and Modeling of Series and Parallel Li-Ion Packs. *Energies,* 10(3). doi: https://doi.org/10.3390/en10030273

Cruz-Manzo, S., Greenwood, P., & Chen, R. (2017). An impedance model for EIS analysis of nickel metal hydride batteries. *Journal of The Electrochemical Society,* 164(7), A1446-A1453. doi: https://doi.org/10.1149/2.0431707jes

Ecker, M., Tran, T. K. D., Dechent, P., Käbitz, S., Warnecke, A., & Sauer, D. U. (2015). Parameterization of a Physico-Chemical Model of a Lithium-Ion Battery. *Journal of The Electrochemical Society,* 162(9), A1836-A1848. doi: https://doi.org/10.1149/2.0541509jes

Fleischer, C., Waag, W., Heyn, H.-M., & Sauer, D. U. (2014). On-line adaptive battery impedance parameter and state estimation considering physical principles in reduced order equivalent circuit battery models. *Journal of Power Sources*, 260, 276-291. doi: https://doi.org/10.1016/j.jpowsour.2014.01.129

Galeotti, M., Cinà, L., Giammanco, C., Cordiner, S., & Di Carlo, A. (2015). Performance analysis and SOH (state of health) evaluation of lithium polymer batteries through electrochemical impedance spectroscopy. *Energy*, 89, 678-686. doi: https://doi.org/10.1016/j.energy.2015.05.148

Gomez, J., Nelson, R., Kalu, E. E., Weatherspoon, M. H., & Zheng, J. P. (2011). Equivalent circuit model parameters of a high-power Li-ion battery: Thermal and state of charge effects. *Journal of Power Sources*, 196(10), 4826-4831. doi: https://doi.org/10.1016/j.jpowsour.2010.12.107

Gong, X., Xiong, R., & Mi, C. C. (2015). Study of the Characteristics of Battery Packs in Electric Vehicles With Parallel-Connected Lithium-Ion Battery Cells. *IEEE Transactions on Industry Applications*, 51(2), 1872-1879. doi: https://doi.org/10.1109/tia.2014.2345951

Hang, T., Mukoyama, D., Nara, H., Takami, N., Momma, T., & Osaka, T. (2013). Electrochemical impedance spectroscopy analysis for lithium-ion battery using Li4Ti5O12 anode. *Journal of Power Sources*, 222, 442-447. doi: https://doi.org/10.1016/j.jpowsour.2012.09.010

Huang, J., Li, Z., Liaw, B. Y., & Zhang, J. (2016). Graphical analysis of electrochemical impedance spectroscopy data in Bode and Nyquist representations. *Journal of Power Sources,* 309, 82-98. doi: https://doi.org/10.1016/j.jpowsour.2016.01.073

Itagaki, M., Honda, K., Hoshi, Y., & Shitanda, I. (2015). In-situ EIS to determine impedance spectra of lithium-ion rechargeable batteries during charge and discharge cycle. *Journal of Electroanalytical Chemistry*, 737, 78-84. doi: https://doi.org/10.1016/j.jelechem.2014.06.004

Jaguemont, J., Boulon, L., & Dube, Y. (2016). Characterization and Modeling of a Hybrid-Electric-Vehicle Lithium-Ion Battery Pack at Low Temperatures. *IEEE Transactions on Vehicular Technology,* 65(1), 1-14. doi: https://doi.org/10.1109/tvt.2015.2391053

Jaguemont, J., Boulon, L., & Dube, Y. (2016). A comprehensive review of lithium-ion batteries used in hybrid and electric vehicles at cold temperatures. *Applied Energy*, 164, 99-114. doi: https://doi.org/10.1016/j.apenergy.2015.11.034

Leng, F., Wei, Z., Tan, C. M., & Yazami, R. (2017). Hierarchical degradation processes in lithium-ion batteries during ageing. *Electrochimica Acta*, 256, 52-62. doi: https://doi.org/10.1016/j.electacta.2017.10.007

Moralı, U., & Erol, S. (2020). 18650 lityum-iyon ve 6HR61 nikel-metal hidrit tekrar şarj edilebilir pillerinin elektrokimyasal empedans analizi. *Gazi Üniversitesi Mühendislik Mimarlık Fakültesi Dergisi,* 35(1), 297-310. doi: https://doi.org/10.17341/gazimmfd.463280

Nelatury, S. R., & Singh, P. (2004). Equivalent circuit parameters of nickel/metal hydride batteries from sparse impedance measurements. *Journal of Power Sources,* 132(1-2), 309-314. doi: https://doi.org/10.1016/j.jpowsour.2003.12.013

Orazem, M. E., & Tribollet, B. (2017). *Electrochemical impedance spectroscopy*. New Jersey, USA: John Wiley & Sons.

Raijmakers, L. H. J., Danilov, D. L., van Lammeren, J. P. M., Lammers, M. J. G., & Notten, P. H. L. (2014). Sensorless battery temperature measurements based on electrochemical impedance spectroscopy. *Journal of Power Sources*, 247, 539-544. doi: https://doi.org/10.1016/j.jpowsour.2013.09.005

Westerhoff, U., Kurbach, K., Lienesch, F., & Kurrat, M. (2016). Analysis of Lithium-Ion Battery Models Based on Electrochemical Impedance Spectroscopy. *Energy Technology*, 4(12), 1620-1630. doi: https://doi.org/10.1002/ente.201600154

Xie, Y., Li, J., & Yuan, C. (2014). Mathematical modeling of the electrochemical impedance spectroscopy in lithium ion battery cycling. *Electrochimica Acta,* 127, 266-275. doi: https://doi.org/10.1016/j.electacta.2014.02.035